Special Feature: Design of High-power Lithium-ion Batteries with Long Operational Life

Research Report

XAFS and XRD Studies on Thermal Decomposition Behavior of Cathode Materials for Lithium-ion Batteries

Takamasa Nonaka, Yoshinari Makimura and Chikaaki Okuda

Report received on Aug. 2, 2017

ABSTRACT In order to investigate the thermal decomposition behavior of cathode materials for Li-ion batteries, two instruments that operate at elevated temperatures have been developed. One is a conversion-electron-yield X-ray absorption fine structure (CEY-XAFS) detector, while the other is an apparatus for simultaneous measurements of XAFS and X-ray diffraction (XRD) in transmission-mode. Both instruments enable measurements with a sample temperature that can be controlled to be from room temperature up to 450°C. We used these instruments to examine $LiNi_{0.75}Co_{0.15}Al_{0.05}Mg_{0.05}O_2$ cathode material at 0% state of charge (SOC) and 50% SOC to explore chemical and structural changes that occur during heating in the absence of an electrolyte. The combination of surface-sensitive CEY-XAFS and bulk-sensitive transmission-mode XAFS showed that the reduction of Ni and Co ions begins at the surface of the cathode particle at around 150°C, and propagates inside the particle upon further heating. XRD showed that during heating up to 450°C, the original layered structure collapses and turns into spinel and rock-salt structures which contain divalent Ni and Co ions. These results demonstrate the capability of the developed instruments to obtain vital information for safely employing this cathode material in Li-ion batteries.

KEYWORDS X-ray Absorption Spectroscopy, X-ray Diffraction, Synchrotron Radiation, Li-ion Battery, Thermal Decomposition, Cathode

1. Introduction

Li-ion batteries have the potential risk of temperature increases due to various reasons such as internal short circuiting and severe overcharging. In a worst-case scenario, the internal temperature increase results in thermal runaway accompanied by abnormal heat generation. Thus, to use Li-ion batteries safely and to develop safer batteries, it is vitally important to understand the mechanism of the exothermic reactions that lead to thermal runaway. Although the exothermic reactions in Li-ion batteries are complicated and their exact details remain unresolved, it has been proposed that cathode materials contribute critically to the overall heat generation in batteries. For instance, it has been reported that $LiNi_{0.8}Co_{0.15}Al_{0.05}O_2$ (NCA)[1,2] exothermically decomposes at high temperatures accompanied by oxygen liberation.[3] The aim of this study was to develop and establish analytical methods to elucidate the detailed mechanisms of the thermal decomposition of cathode materials.

One of the necessary features of such analytical methods is that measurements under high temperatures should be possible, because cathode materials at elevated temperatures are unstable and analyses "after" heating will not provide accurate information on the chemical and structural changes in the cathode materials. Another requirement for these analytical methods is surface selectivity. Cathode materials are typically composed of secondary particles with sizes ranging from a few micrometers to over 10 μm, and the surfaces of these particles can directly contact the electrolyte. Hence, the decomposition of the cathode materials is expected to begin at the surface of the cathode particles. Analyzing cathodes using a surface-sensitive probe is necessary to obtain the exact onset temperature for the chemical and structural changes, which is an important parameter for characterizing thermal decomposition.

X-ray absorption fine structure (XAFS) is an analytical tool allowing in situ investigation of the chemical states and the local environment of atoms in materials, and is widely used in the field of battery research. In particular, the combination of surface-sensitive

conversion-electron-yield XAFS (CEY-XAFS)[4-6] with bulk-sensitive transmission-mode XAFS provides a powerful method to explore the details of chemical and structural changes of cathode materials. In a previous study, we applied this combined techniques to NCA cathode materials after cycling tests and aging tests at 60°C, and elucidated that electrochemically inactive NiO-like layers grow predominantly at the surface of cathode particles.[7,8] These results, however, were obtained at room temperature; a CEY-XAFS detector equipped with a temperature controller is required to perform high-temperature observations of the thermal decomposition of cathode materials. In addition to these XAFS-related techniques, X-ray diffraction (XRD) is also useful for investigating the long-range-order structures of cathode materials; one can expect that simultaneous XAFS and XRD measurements can provide in-depth and complementary information about the changes in the cathode materials.

To meet the above requirements for the analytical method, in this study, we developed two instruments for high-temperature measurements. The first is a temperature-controllable CEY-XAFS detector, and the second is an apparatus for simultaneous measurements of transmission XAFS and XRD with temperature control. Both instruments enable carrying out measurements with a sample temperature that is controllable from room temperature up to 450°C. To demonstrate their usefulness, we applied the instruments to a $LiNi_{0.75}Co_{0.15}Al_{0.05}Mg_{0.05}O_2$ (NCA-Mg) cathode material,[9] the stability of which is improved by Mg-substitution for Ni in the NCA cathode material, and examined the behavior of thermal decomposition in the process of being heated up to 450°C. In this paper, details of the developed instruments and the results of their application to the NCA-Mg cathode material are presented.[10,11]

2. Instrumentation

Figure 1(a) shows a schematic drawing of the temperature-controllable CEY-XAFS detector. The main body, which is made of aluminum, has a drawer-type lid that is equipped with a carbon electrode and a temperature controller. A machined-ceramic lining is placed in the interior of the main body for thermal insulation. The sample is mounted on the carbon electrode with a ceramic holding plate. The other carbon electrode, which has a He gas inlet, is located at the upper part of the main body. Helium gas is supplied to the main body at a flow rate of 0.5 L/min after being heating to the same temperature as the sample using a hose-type heater, so that room-temperature He gas does not cool the sample. The main body has a Kapton window through which incident X-rays can penetrate. Figure 1(b) shows a cross-sectional view of the interior of the detector with the lid closed. The upper and lower electrodes are situated oppositely at a distance of 15 mm, and a high voltage of 1 kV is applied between the electrodes. The sample temperature is controlled to be between room temperature and 450°C with a ceramic heater embedded under the lower electrode and a thermocouple. The He atoms are ionized by Auger electrons that are emitted from the sample surface by X-ray irradiation, and the resultant He ions are collected by the lower electrode. The probing depth of CEY-XAFS is approximately equal to the Auger electron escape depth and is estimated to be approximately 90 nm for Ni K-edge CEY-XAFS of the

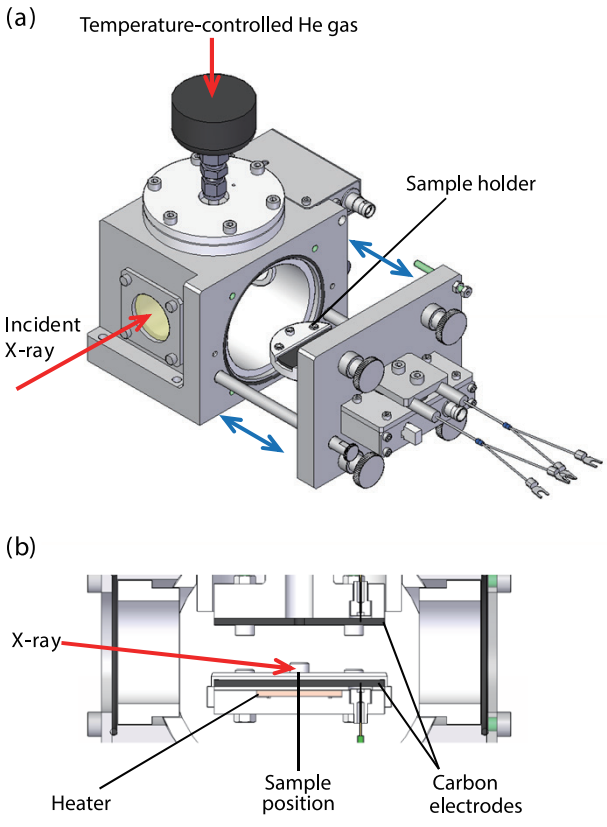

Fig. 1 (a) Schematic drawing of CEY-XAFS detector equipped with temperature controller. (b) Cross-sectional view of the detector interior.

NCA-Mg cathode material used in this study.[7]

Figure 2 shows a schematic drawing of the apparatus for simultaneous measurements of transmission XAFS and XRD with temperature control. Two machined-ceramic box-like bodies clamp and hold the sample. At the parts of the box-like bodies that touch the sample, 5-mm-diameter holes are made through which hot air emitted from two heat guns is injected towards the sample. With these heat guns and thermocouples placed near the sample, the sample temperature can be controlled between room temperature and 450°C. The box-like bodies have 5-mm-width slits sealed by Kapton films, enabling incident X-rays, transmitted X-rays, and diffracted X-rays to pass through the bodies. The transmission XAFS and XRD data can be obtained almost simultaneously by collecting transmitted X-rays and diffracted X-rays with an ionization chamber and a two-dimensional X-ray detector, respectively.

3. Experimental

Cathode sheets taken from 18650-type cells were used as samples. The cells consisted of a cathode sheet, an anode sheet, a 1 M $LiPF_6$ electrolyte dissolved in a solvent of 3:4:3 (by volume) EC (ethylene carbonate)/DEC (dimethyl carbonate)/EMC (ethyl methyl carbonate), and a microporous polypropylene separator. The cathode sheet was a thin Al metal foil coated on both sides with approximately 20-µm-thick electrode mixtures composed of 85 wt% NCA-Mg, 10 wt% carbon black, and 5 wt% polyvinylidene fluoride binder. The anode sheet was a thin Cu metal foil coated on both sides with 95 wt% graphite and 5 wt% polyvinylidene fluoride binder.

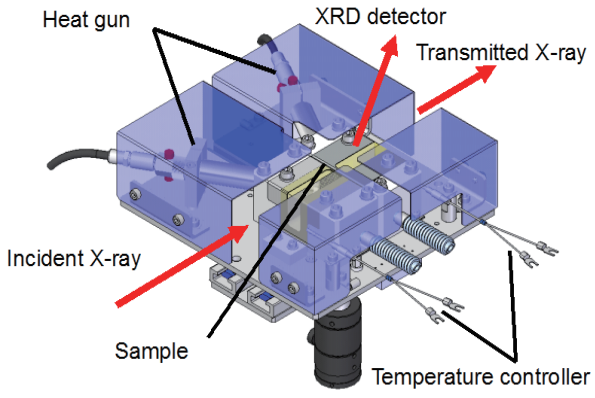

Fig. 2 Schematic drawing of the apparatus for simultaneous measurements of transmission XAFS and XRD with temperature control.

The states of charge (SOC) of the cells were adjusted to be 0% and 50%, which corresponded to potentials (vs. Li^+/Li) of 3.006 V and 3.679 V, and compositions of x = 0.06 and 0.37 in $Li_{1-x}Ni_{0.75}Co_{0.15}Al_{0.05}Mg_{0.05}O_2$, respectively. The compositions were determined using inductively coupled plasma-atomic emission spectroscopy. The cells were disassembled in an Ar-filled glove box to obtain the cathode sheets. After cutting the cathode sheets to a size of 20 × 20 mm^2, they were rinsed with DMC solution to remove the electrolyte and then dried under an Ar atmosphere to yield samples for measurement.

XAFS and XRD measurements were performed at the BL33XU beamline (Toyota beamline)[12,13] at SPring-8. This beamline offers quick-scanning XAFS measurements realized by combining a servo-motor-driven Si channel-cut monochromator with a tapered undulator.[14] X-rays with an energy range of 7.4-9.5 keV were generated by tuning the taper ratio of the undulator gap, and were employed for the measurements with sufficient bandwidth to simultaneously measure Co and Ni K-edge XAFS. Si(111) channel-cut crystal cooled with liquid nitrogen was used to monochromatize the X-rays. Higher harmonics of the X-rays were rejected using a pair of Rh-coated Si mirrors. The beam size at the sample position was 0.5 (H) mm × 1.2 (W) mm. For XRD measurements, X-rays with an energy of 8.0 keV (λ = 1.55 Å) were used. Two-dimensional diffraction patterns were recorded with a flat-panel sensor (Hamamatsu Photonics, C10158DK), which has 2376 × 2376 pixels with a pixel size of 50 µm × 50 µm. The sensor was installed about 166 mm away from the sample and with an elevation angle of 34°; this geometry corresponded to a diffraction angle range of 14–55° and an average angular resolution of 0.017°. The exact diffraction angles were calculated using a Ni metal foil as the standard material. Both CEY-XAFS and transmission XAFS and XRD data were collected at temperatures ranging from room temperature to 450°C in 50°C steps and also after cooling to 50°C. The total measurement time for the Co and Ni K-edge XAFS was 350 s. For each XRD measurement, X-ray images with an exposure time of 1 second were recorded 100 times, and the images were integrated

into one averaged image. The two-dimensional XRD images were transformed into one-dimensional XRD patterns using the ImageJ software.[15]

4. Results and Discussion

Figure 3(a) shows representative Ni K-edge X-ray absorption near-edge structure (XANES) spectra for NCA-Mg at 50% SOC measured in the bulk-sensitive transmission-mode and the surface-sensitive CEY-mode. As temperature increases, the entire profile of the spectrum shifts toward lower energies, regardless of the probing mode, indicating that the average valence of Ni decreases. However, the energy shift upon heating appears to be dependent on the probing mode. In order to clarify the differences of the energy shift, the energy at a half-step height (i.e., where the normalized absorbance is 0.5) was calculated for each spectrum. It is generally considered that this value can be used to roughly estimate the average oxidation state of Ni ions.[16] The difference between the energy at the half-step height for the sample and that for a Ni metal foil (edge shift) is plotted as a function of heating temperature in Fig. 3(b). The edge shifts for NiO and $LiNiO_2$ are also shown for comparison in the figure.

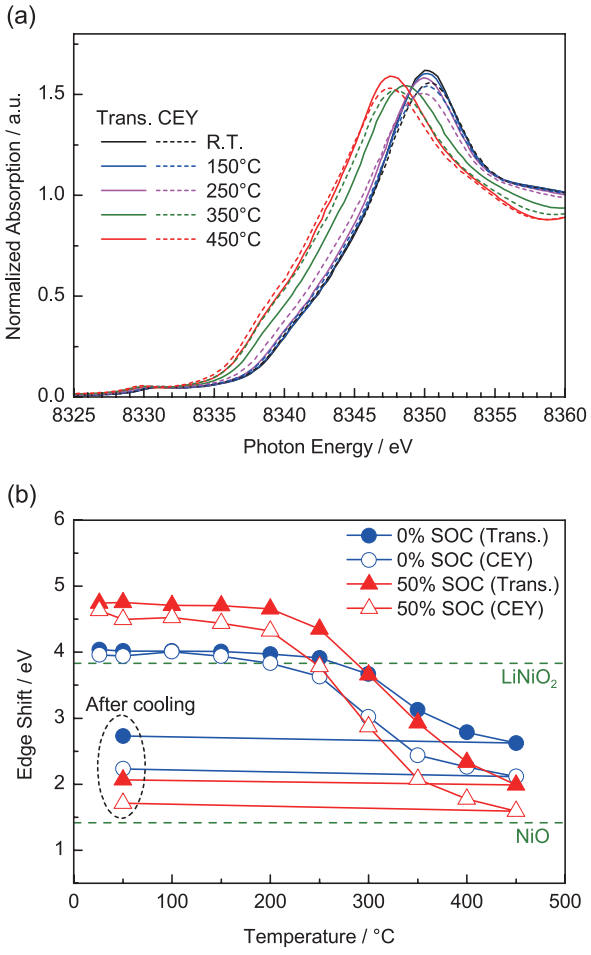

Fig. 3 (a) Representative Ni K-edge XANES spectra for $LiNi_{0.75}Co_{0.15}Al_{0.05}Mg_{0.05}O_2$ at 50% SOC measured in transmission-mode (Trans.) and CEY-mode (CEY). (b) Temperature dependence of Ni K-edge shifts measured at half the step height in the spectra. Edge shifts are calculated as the difference between the edge positions of the samples and that of Ni metal foil. Edge shifts for NiO and $LiNiO_2$ are shown for comparison.

As can be seen, the edge shift for 0% SOC of the transmission-mode at room temperature is close to that for $LiNiO_2$. The edge shift begins to decrease gradually at around 200°C and reaches the median value for $LiNiO_2$ and NiO, when heated to 450°C. The interpretation for this is that Ni ions, which are originally trivalent at room temperature, are partially reduced to divalent during heating. Meanwhile, for 0% SOC of the surface-sensitive CEY-mode, the average Ni valence begins to decrease at a temperature about 50°C lower than the onset-temperature determined in the transmission-mode. This indicates that the reduction of Ni ions begins at the surface of the cathode particles, and the reduction then propagates inside the particles with further heating. In the case of 50% SOC, the edge shift at room temperature is higher than that for 0% SOC, because some portion of trivalent Ni ions becomes tetravalent upon charging the cell. The average Ni valence for 50% SOC decreases gradually during heating and reaches a value closer to that for NiO than for 0% SOC. It is considered that the reduction of Ni ions at high temperatures occurs because a portion of Ni^{4+} ions migrates into the Li layer, where Ni^{4+} turns into Ni^{2+}.[17] For this reason, 50% SOC, which contains a larger amount of Ni^{4+} than 0% SOC, is reduced to a greater extent. As in the case of 0% SOC, the onset-temperature for reduction measured in the CEY-mode is about 50°C lower than that measured in the transmission-mode. The edge shifts for the sample cooled down to 50°C after heating to 450°C are almost the same as those measured at 450°C, indicating that the reduction of Ni atoms is irreversible when the sample is heated up to 450°C.

Representative Co K-edge XANES spectra for NCA-Mg at 50% SOC and the edge shifts obtained by the same procedure as the Ni K-edge are shown

in **Figs. 4**(a) and (b), respectively. The edge shifts were calculated as the difference between the edge positions of the samples and that of Co metal foil. The edge shifts for CoO, Co_3O_4 and $LiCoO_2$ are also shown for comparison. The edge shifts at room temperature are close to those for $LiCoO_2$ and are independent of the SOC. This is because in the SOC range of 0–50%, Co ions do not contribute to charge compensation of NCA-Mg upon charging, maintaining their trivalent states.[18] The average Co valence begins to decrease at around 200°C as observed in the Ni K-edge spectra. During heating above 200°C, the oxidation state for the CEY-mode is lower than that for the transmission-mode, and that for 50% SOC is lower than that for 0% SOC. After heating up to 450°C, the oxidation state of Co does not return to the original value, even when cooled to 50°C. These findings suggest that as in the case of Ni, the reduction of Co ions begins at the surface of the cathode particles and then proceeds irreversibly. However, the extent of the reduction of Co ions is much smaller than that of Ni ions. This is attributed to the more thermally stable local structure around Co than that around Ni, and it is harder to reduce Co^{3+} ions than Ni^{3+} ions.[19-22]

Figure 5(a) shows XRD patterns of NCA-Mg at 0% SOC during heating, up to 450°C, and after cooling down to 50°C. At room temperature, the observed

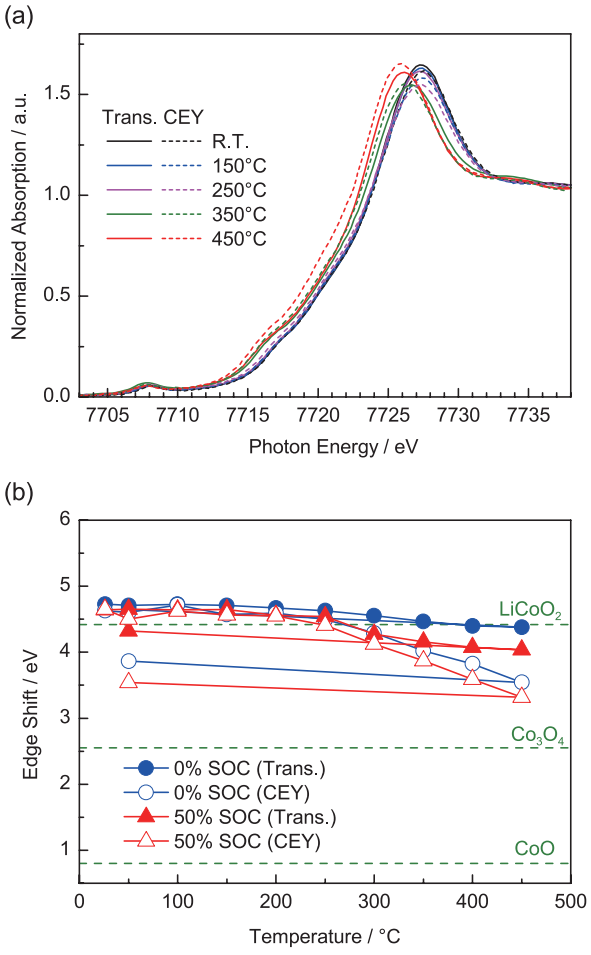

Fig. 4 (a) Representative Co K-edge XANES spectra for $LiNi_{0.75}Co_{0.15}Al_{0.05}Mg_{0.05}O_2$ at 50% SOC measured in transmission-mode (Trans.) and CEY-mode (CEY). (b) Temperature dependence of the Co K-edge shifts measured at half step height in the spectra. Edge shifts are calculated as the difference between the edge positions of the samples and that of Co metal foil. Edge shifts for CoO, Co_3O_4 and $LiCoO_2$ are shown for comparison.

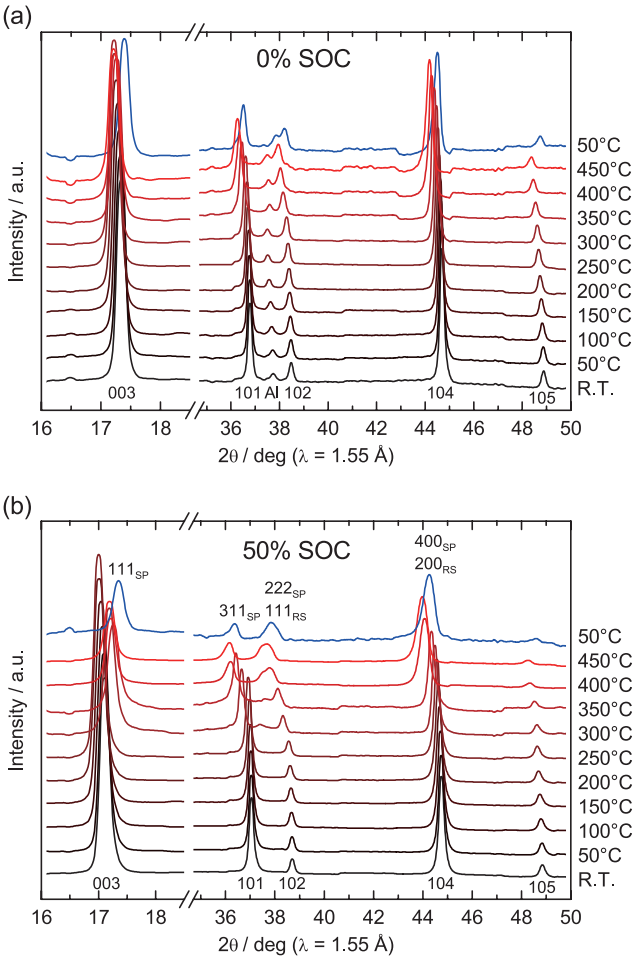

Fig. 5 XRD patterns for $LiNi_{0.75}Co_{0.15}Al_{0.05}Mg_{0.05}O_2$ at (a) 0% SOC and (b) 50% SOC during heating up to 450°C and after cooling down to 50°C (the topmost pattern). The subscripts SP and RS denote spinel and rock-salt structure, respectively.

diffraction lines can be indexed based on the *R-3m* space group, and these are consistent with the layered structure of α-$NaFeO_2$. As the temperature increases, the entire XRD pattern shows little change except for slight peak shifts to lower angles due to thermal expansion. For the pattern obtained at 50°C after heating to 450°C, the width of each peak broadens and the relative intensities of the (003), (101), and (105) peaks decrease compared to the room temperature results. This suggests that the original layered structure is basically maintained during heating and is partly transformed into a different phase, which is most likely to be a spinel phase (*Fd3m*), as described later.

Meanwhile, the XRD patterns at 50% SOC (Fig. 5(b)) show obvious peak shifts and broadenings in the temperature range above 300°C. The pattern obtained after heating to 450°C is significantly different from that obtained at room temperature. Four distinct peaks can be assigned to the (111), (311), (222), and (400) peaks of the spinel phase (*Fd3m*), and two peaks at the higher-angle side can also be assigned to the (111) and (200) peaks of a rock-salt phase (*Fm3m*). It has been reported that in the case of the NCA cathode material, the original layered structure first transforms into the spinel structure upon heating and then converts to the rock-salt structure with further heating.[3,20,23-25] Similar phase transitions are believed to occur in our NCA-Mg cathode materials. These XRD findings are consistent with the XANES results since the spinel and rock-salt phases contain divalent Ni and Co ions.

Our XAFS and XRD findings elucidated the thermal decomposition behavior of the NCA-Mg at 50% SOC to be as follows. First, when heated to around 150-200°C, the reduction of Ni and Co begins at the surface of the cathode particles. At this stage, no distinguishable changes are observed in the transmission-mode XAFS and XRD results, which reflect the bulk-averaged information. Second, upon further heating, the reduction gradually proceeds inwards from the surface, and finally at around 300°C, the long-range-order structure converts from the layered structure into the spinel and rock-salt structures. These chemical and structural changes at elevated temperatures should be accompanied by the release of oxygen from the cathode particles. We consider that the thermal transitions identified in this study are essentially identical to the changes caused by cycling and aging tests at 60°C that we previously observed in the NCA cathode material, i.e., that NiO-like layers grow at the surface of the cathode, which is accompanied by oxygen loss.[7,8,26] Heating at higher temperatures than those in the previous study likely accelerates the progress of the transition.

5. Conclusion

In order to study the thermal decomposition of cathode materials for Li-ion batteries, we developed a CEY-XAFS detector and the apparatus for simultaneous measurements of transmission XAFS and XRD, both of which can control the sample temperature between room temperature and 450°C. This combined technique successfully revealed the thermal decomposition mechanism of the NCA-Mg cathode material at 0% and 50% SOC in the absence of the electrolyte. At around 150-200°C, Ni and Co ions begin to be reduced at the surface of the cathode particles, and the reduction then propagates inside the particle with further heating. In the process of being heated up to 450°C, the original layered structure turns gradually into spinel and rock-salt structures which contain divalent Ni and Co ions. These changes are irreversible and are more obvious for 50% SOC than for 0% SOC, and the fraction of reduced Ni ions is larger than that of reduced Co ions.

The results of this study are important for determining safe operating conditions for Li-ion batteries that contain the NCA-Mg cathode material. Moreover, applying the analytical techniques developed in this study to various battery operating conditions or batteries composed of different materials will provide crucial information that can lead to the safe use of the batteries and the development of safer batteries. For example, we studied the effect of the electrolyte in the thermal decomposition of NCA-Mg using the transmission XAFS and XRD apparatus developed in this study, and found that the decomposition reaction is accelerated in the presence of the electrolyte.[10]

References

(1) Weaving, J. S. et al., *J. Power Sources*, Vol. 97-98 (2001), pp. 733-735.
(2) Itou, Y. and Ukyo Y., *J. Power Sources*, Vol. 146 (2005), pp. 39-44.
(3) Bang, H. J. et al., *J. Electrochem. Soc.*, Vol. 153, No. 4 (2006), pp. A731-A737.
(4) Shevchik, N. J. and Fischer, D. A., *Rev. Sci. Instrum.*, Vol. 50, No. 5 (1979), pp. 577-581.

(5) Schroeder, S. L. M. et al., *Surf. Sci. Lett.*, Vol. 324, No. 2-3 (1995), pp. L371-L377.
(6) Takahashi, M. et al., *J. Synchrotron Rad.*, Vol. 6 (1999), pp. 222-224.
(7) Nonaka, T. et al., *J. Electrochem. Soc.*, Vol. 154, No. 4 (2007), pp. A353-A358.
(8) Sasaki, T. et al., *J. Electrochem. Soc.*, Vol. 156, No. 4 (2009), pp. A289-A293.
(9) Kondo, H. et al., *J. Power Sources*, Vol. 174, No. 2 (2007), pp. 1131-1136.
(10) Makimura, Y. et al., *ECS Electrochem. Lett.*, Vol. 3, No. 6 (2014), pp. A66-A68.
(11) Nonaka, T. et al., *J. Power Sources*, Vol. 325 (2016), pp. 79-83.
(12) Hirose, Y., *SPring-8 Research Frontiers 2009* (2010), p. 170.
(13) Nonaka, T. et al., *AIP Conf. Proc.*, Vol. 1741, No. 1 (2016), 030043.
(14) Nonaka, T. et al., *Rev. Sci. Instrum.*, Vol. 83, No. 8 (2012), 083112.
(15) Schneider, C. A. et al., *Nat. Methods*, Vol. 9, No. 7 (2012), pp. 671-675.
(16) Mansour, A. N. et al., *J. Electrochem. Soc.*, Vol. 147, No. 6 (2000), pp. 2104-2109.
(17) Arai, H. et al., *Solid State Ion.*, Vol. 109, No. 3-4 (1998), pp. 295-302.
(18) Nonaka, T. et al., *J. Power Sources*, Vol. 162, No. 2 (2006), pp. 1329-1335.
(19) Lee, K.-K. et al., *J. Electrochem. Soc.*, Vol. 148, No. 10 (2001), pp. A1164-A1170.
(20) Nam, K. W. et al., *Adv. Funct. Mater.*, Vol. 23, No. 8 (2013), pp. 1047-1063.
(21) Wang, L. et al., *Chem. Mater.*, Vol. 19, No. 3 (2007), pp. 543-552.
(22) Kim, Y. et al., *Chem. Mater.*, Vol. 23, No. 24 (2011), pp. 5388-5397.
(23) Yoon, W.-S. et al., *Electrochem. Solid-state Lett.*, Vol. 8, No. 2 (2005), pp. A83-A86.
(24) Yoon, W.-S. et al., *J. Power Sources*, Vol. 163, No. 1 (2006), pp. 219-222.
(25) Wu, L. et al., *Chem. Mater.*, Vol. 23, No. 17 (2011), pp. 3953-3960.
(26) Muto, S. et al., *J. Electrochem. Soc.*, Vol. 156, No. 5 (2009), pp. A371-A377.

Takamasa Nonaka
Research Field:
- Materials Analysis Using Synchrotron Radiation

Academic Degree: Dr.Eng.
Academic Society:
- The Japanese Society for Synchrotron Radiation Research

Award:
- Promotion Award from the Ceramic Society of Japan (2008)

Yoshinari Makimura
Research Field:
- Solid-State Chemistry and Electrochemistry of Inorganic Compounds for Energy Storage Devices

Academic Degree: Ph.D.
Academic Societies:
- The Electrochemical Society of Japan
- The Electrochemical Society

Chikaaki Okuda
Research Field:
- Development of Electrode Structure and Process for Li-ion Batteries

Academic Society:
- The Electrochemical Society of Japan